Environmental Science and Pollution Research (2019) 26:32836–32851
https://doi.org/10.1007/s11356-019-06374-6

RESEARCH ARTICLE

Effects of aquatic phototrophs on seasonal hydrochemical, inorganic, and organic carbon variations in a typical karst basin, Southwest China

Ping'an Sun[1,2] · Shiyi He[1] · Yaqiong Yuan[1] · Shi Yu[1] · Cheng Zhang[1]

Received: 11 April 2019 / Accepted: 29 August 2019 / Published online: 9 September 2019

Abstract

Karst processes play an important role in the global carbon cycle. Aquatic phototrophs can transform bicarbonate, which is mainly derived from the weathering of carbonates, into organic carbon. Carbonate mineral weathering coupled with aquatic photosynthesis can be considered a stable and durable carbon sink process. In this study, we addressed seasonal variations in water chemistry in the Lijiang River Basin, which is a typical karst basin, through a comprehensive geochemical study of the river water in four seasons. The parameters were measured in situ, including major ions and isotopes of inorganic and organic carbon. The results showed that (1) DIC was mainly derived from the weathering of carbonates; (2) the transformation from bicarbonate to organic carbon by aquatic phototrophs was evident, and the water chemistry changed, especially in spring and autumn and in the mainstream from Guilin to Yangshuo, which benefited the growth of aquatic phototrophs; and (3) the organic carbon derived from bicarbonates by aquatic phototrophs was nearly half the total organic carbon and 8% of the dissolved inorganic carbon. These results imply that aquatic phototrophs in karst basins can significantly stabilize carbon originating from carbonate rock weathering processes in karst areas.

Keywords Karst processes · Hydrochemistry · Stable carbon isotope · Aquatic phototrophs · Lijiang River Basin

Introduction

Rivers play an important role in biogeochemical reactions involving the global carbon cycle by linking several major carbon reservoirs, including the atmosphere, biosphere, terrestrial geosphere, and ocean. The chemical compositions of rivers can reflect weathering, human activities and biological functions in basins (Gaillardet et al. 1999; Hindshaw et al. 2011; Li et al. 2011b). Previous studies have shown that the weathering of carbonates is a rapid and sensitive reaction process (Liu and Dreybrod 1997; Liu et al. 2007; Raymond et al. 2008). Therefore, the ion content is remarkably higher in carbonate terrains and mixed silicate than in silicate terrains, which are dominated by bicarbonate and calcium. The weathering of carbonates contributes most to carbonate terrains, but the different forms of carbonate weathering have completely different implications for the global carbon cycle. Carbonate mineral dissolution by carbonic acid may represent a net, but short time, atmospheric carbon dioxide (CO_2) sink, as primary productivity consumes dissolved inorganic carbon (DIC) (Martin 2017). Alternatively, carbonate minerals dissolved by sulfuric and nitric acids may represent an atmospheric source of CO_2 with no rapid balancing atmospheric sink (Perrin et al. 2008; Torres et al. 2014; Martin 2017). The weathering of carbonates by sulfuric and nitric acid is common in karst areas (Li et al. 2008; Perrin et al. 2008), including the Lijiang River Basin (Yu et al. 2016). Therefore, the forms of carbonate weathering should be distinguished first in karst basins.

As a net atmospheric CO_2 sink, bicarbonate sourced from carbonate weathering by carbonic acid must be used by aquatic phototrophs and transformed into organic carbon in inland waters (Liu et al. 2011). Bicarbonate uptake by aquatic

Responsible editor: Philippe Garrigues

✉ Ping'an Sun
safesun@163.com

[1] Key Laboratory of Karst Dynamics, Ministry of Natural Resources & Guangxi, Institute of Karst Geology, Chinese Academy of Geological Sciences, Guilin 541004, China

[2] State Key Laboratory of Biogeology and Environmental Geology, School of Environmental Studies, China University of Geosciences, Wuhan 430074, China

phototrophs has been found both in the laboratory (Liu et al. 2010; Wu et al. 2012; Wang et al. 2013) and in the field, in the outflow of springs and subterranean rivers, for example, Zhang et al. (2012a); Chen et al. (2014b); Pu et al. (2017). Atmospheric CO_2 uptake by interactions among water, carbonate minerals, dissolved CO_2, and aquatic phototrophs on land has been estimated to be as large as 0.5 $PgC{\cdot}a^{-1}$ (Liu et al. 2018). The autochthonous organic carbon that is transformed from bicarbonate by aquatic phototrophs via photosynthesis in the surface water system is approximately 0.27 $PgC{\cdot}a^{-1}$ (Liu et al. 2018), which can be seen as a net atmospheric CO_2 sink and a large fraction of the net terrestrial residual sink (i.e., 0.8~1.2 $PgC{\cdot}a^{-1}$) (Ciais et al. 2013). Therefore, revealing the source of bicarbonate and the transformation from bicarbonate to organic carbon in karst basins is critical for understanding carbon cycling and its role in regional and global carbon budgets.

This study assessed the concentrations of DIC sourced from carbonate weathering by carbonic acid, sulfuric or nitric acid, and silicate weathering variations in different seasons. The bicarbonate-transformed organic carbon (OC) in riverine OC was evaluated. This assessment was based on data collected from a subtropical karst basin (Lijiang River Basin) located in Southwest China. This study comprehensively assessed the geochemistry of river waters in four seasons and included water chemistry measurements and inorganic and OC isotope analyses. The analytical results combined with the geological setting will help to improve evaluations of DIC sources and riverine OC and improve the understanding of the transformation from bicarbonate to OC in different seasons.

Study area and methods

Lijiang River Basin characteristics and hydrology

The Lijiang River Basin is located in the northeastern part of Guangxi Zhuang Autonomous Region, China (Fig. 1), which has a catchment of 5039 km^2. This area is located in the middle and upper reaches of the Guijiang River, which is a secondary tributary of the Pearl River. As shown in Fig. 1, the Lijiang River Basin has a mixed carbonate and silicate terrain. Bare karst areas, where carbonates are exposed (blue in Fig. 1), and covered karst areas, where carbonates are covered by Quaternary material (yellow in Fig. 1), are widely distributed in the Lijiang River Basin, especially in the middle and southern areas, and cover nearly half of the total basin area (Fig. 1). Evaporates do not exist in the study area, and the remaining areas are nonkarst (blank in Fig. 1), mainly consisting of silicate rocks such as granite and clastic rocks. The ratio of karst areas (including bare and covered karst areas) in each sampling site was calculated based on a geologic map, and the results are shown in Table 1.

The nine sampling locations are shown in Table 1 and Fig. 1. Six locations were located on the mainstream from upstream to downstream, with the stream gradient decreasing and the karst area increasing (Table 1). Three other sites were located on tributaries with different hydrology characteristics (Table 1 and Fig. 1). Site HJ was located near the Cat Mountain nature protection area, and this basin is mostly covered by forest. Site DR was located in the lower reaches of site HJ, and several villages are located between sites HJ and DR. The cities and towns in the basin are mainly located in areas covered by Quaternary material. Because the soil is thicker in covered karst areas than in bare karst areas, farmland is also mainly located in this area. Thus, sites LQ and CT are influenced by industrial and agricultural activities. Site GL was located in the city of Guilin, which is substantially affected by human activities. Sites GY, XP, and YL were in areas that are influenced by tourist activities, especially during the peak tourism seasons of January, February, July, and August, which are the winter and summer vacation times in China. Site YS was located in the county of Yangshuo, which is influenced by industrial and agricultural activities. Aquatic phototrophs such as phytoplankton and submerged plants can be found along the river and flourish in the mainstream from Guilin to Yangshuo (sites GL, GY, XP and YS) and the tributary of site LQ. The phytoplanktons were mainly Bacillariophyta and Chlorophyta, and the dominant species were *S. tephanodiscus*, *C. pyrenoidosa*, *N. rhynchocephal*, *N. exigua*, *C. Bodanica*, *S. quadricanda*, and *S. ulna* (Zhou et al. 2014). The dominant species of submerged plants were *Vallisneria spiralis* and *Hydrilla verticillata* in the Lijiang River (Chen et al. 2014a).

Sampling and analytical approaches

Water samples from these nine sampling locations were collected in April, July, and October 2015, and January 2016. The sampling locations are shown in Fig. 1 and Table 1. Temperature, pH, specific conductance (SpC), dissolved oxygen (DO), chlorophyll, and turbidity were measured in situ with a multiparameter analyzer (Manta2™ 4.0, Eureka, USA). Alkalinity (HCO_3^- and CO_3^{2-}) was determined with an alkalinity test (MColortest™, Merck KGaA, Germany) in situ. Samples for K^+, Na^+, Ca^{2+}, and Mg^{2+} analysis were filtered through 0.22-μm membrane filters, acidified with ultrapurified 6 M HNO_3 to a pH < 2, and then determined by inductively coupled plasma-optical emission spectrometry (ICP-OES) (isotope ratio mass spectrometer (IRIS), Intrepid II XSP, Thermo Fisher Scientific, USA). Anions (F^-, Cl^-, NO_3^-, and SO_4^{2-}) were measured by ionic chromatography (861 advanced compact IC Metrohm, Switzerland). The dissolved silica (Si) concentrations were

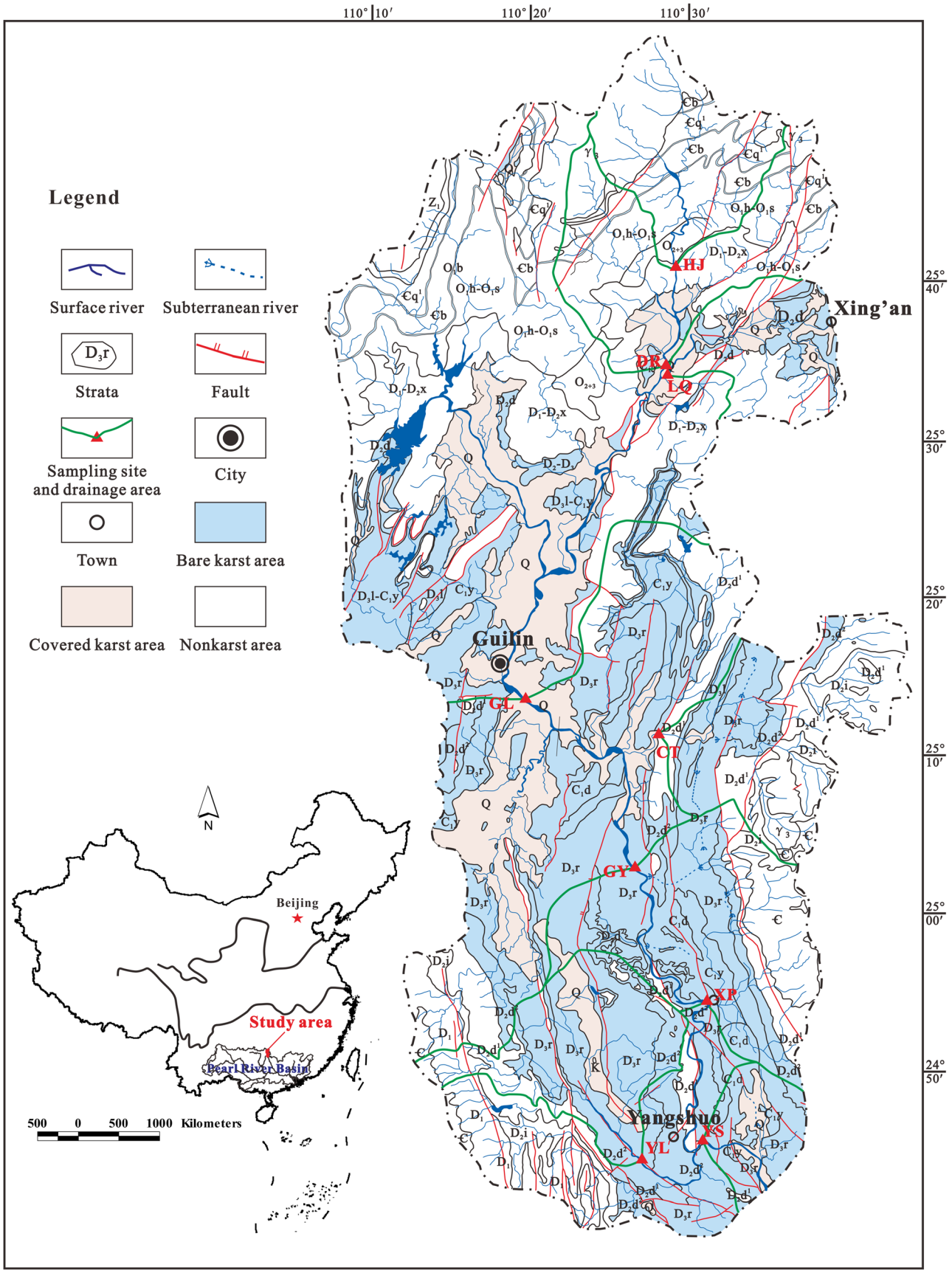

Fig. 1 Sketch map showing the karst type and sampling locations in the Lijiang River Basin

Table 1 Hydrology characteristics of the sampling locations

Sampling location	Area (km^2)	Ratio of karst area (%)	Stream gradient (m km^{-1})	Human activities
HJ (mainstream)	313	2	71.00	Forests
LQ (tributary)	248	48	5.40	Xing'an town
DR (mainstream)	719	9	3.54	Villages
GL (mainstream)	2745	33	1.14	Guilin city
CT (tributary)	476	36	22.71	Daxu town
GY (mainstream)	4030	43	0.50	Caoping town, tourist area
XP (mainstream)	4480	46	0.46	Xinping town, tourist area
YL (tributary)	346	90	1.58	Tourist area
YS (mainstream)	5039	49	0.49	Yangshuo town

determined by spectrophotometry using the molybdate blue method. The cation, anion, and dissolved silica concentrations were determined at the Water Environmental Laboratory, Institute of Karst Geology.

Samples for the analysis of the carbon isotope composition of DIC ($\delta^{13}C_{DIC}$) were collected in a 30-ml bottle, poisoned with saturated $HgCl_2$ (approximately 0.05 ml), and capped without headspace. Samples for the analyses of total suspended matter (TSM), particulate OC (POC), particulate organic nitrogen (PON), and carbon isotope composition of POC ($\delta^{13}C_{POC}$) were obtained by filtering 500–5000 ml of water on precombusted (4 h at 500 °C) and preweighed glass fiber filters (47-mm GF/F, 0.45-μm nominal pore size) and dried in ambient air. The filtrate was collected for determining the dissolved OC (DOC) and carbon isotope composition of DOC ($\delta^{13}C_{DOC}$).

TSM was calculated by the weight difference before and after filtering. DOC was determined by a total OC analyzer (multi N/C®-3100, Analytikjena, Germany). Samples for the $\delta^{13}C_{DIC}$ analysis were acidified with H_3PO_4 and determined by an IRMS at the Water Environmental Laboratory, Institute of Karst Geology. Samples for the $\delta^{13}C_{DOC}$ determination were analyzed following the GasBench-IRMS method (Lang et al. 2012) at the Water Environmental Laboratory, Institute of Karst Geology. The POC, PON, and $\delta^{13}C_{POC}$ measurements were determined by an elemental analyzer (EA)-IRMS at the Open Laboratory of Ocean & Coast Environmental Geology, Third Institute of Oceanography State Oceanic Administration.

Results

Chemical compositions

The solution parameters, including pH, temperature, EC, DO, chlorophyll, and turbidity, and the major and trace element concentrations of the water samples are presented in Table 2. The water samples were mildly alkaline and acidic, with pH values ranging from 6.45 to 8.52. The SpC, DO, chlorophyll, and turbidity were 41.8–348.3 μs cm^{-1}, 6.96–14.76 mg L^{-1}, 0.33–5.10 ng L^{-1}, 1.0–64.0 NTU, respectively.

The total cation charge ($TZ^+ = K^+ + Na^+ + 2Ca^{2+} + 2Mg^{2+}$) ranged from 489 to 3911 μEq (10^{-6} charge equivalent units per liter) with an average of 1870 μEq, and the total anion charge ($TZ^- = F^- + Cl^- + NO_3^- + 2SO_4^{2-} + HCO_3^- + 2CO_3^{2-}$) ranged from 534 to 3691 μEq, with an average of 1838 μEq. Except for the sites HJ and DR which had low total charge (< 1500 μEq), the differences between the charges of the anions and the cations were less than 5%. The TDSs ($TDS = K^+ + Na^+ + Ca^{2+} + Mg^{2+} + F^- + Cl^- + NO_3^- + SO_4^{2-} + HCO_3^- + CO_3^{2-} + Si$) ranged from 48.6 to 198.8 mg L^{-1}, with an average of 149.1 mg L^{-1}. The TZ^+, TZ^-, and TDS results were within the variation found in the Pearl River Basin (Xu and Liu 2007; Qin et al. 2013) and the world's 61 largest rivers (Gaillardet et al. 1999).

Variations in the major ion compositions are shown in the anion and cation ternary diagrams (Fig. 2), and the samples define a narrow range on the ternary diagrams. Ca^{2+} dominated the cation concentrations in these waters, ranging from 59 to 91%, with an average of 78% of the total cation concentration. Mg^{2+} was the second dominant cation, with a concentration between 41 and 364 μmol L^{-1}. The samples from sites HJ and DR, which had low ratios of carbonate rock distribution areas (2% and 9%, respectively), had higher $K^+ + Na^+$ concentrations (Fig. 2a).

HCO_3^- was the dominant anion in the samples, ranging from 54 to 92%, with an average of 78% of the total anion concentration. SO_4^{2-} was the second dominant anion, with a concentration between 36 and 205 μmol L^{-1}. The Cl^- and NO_3^- concentrations were 16–274 μmol L^{-1} and 0–422 μmol L^{-1}, respectively, and the highest values occurred in the winter at site GL. The Si concentrations ranged from 21 to 169 μmol L^{-1}. Similar to the $K^+ + Na^+$ concentrations, the Si concentrations at sites HJ and DR were also high (Fig. 2b).

Table 2 Chemical compositions of the waters in the Lijiang River Basin, Southwest China

Sample number	Date	T (°C)	pH	Ec (μS cm^{-1})	DO (mg L^{-1})	Chlorophyll (ng·L^{-1})	Turbidity (NTU)	K^+	Na^+	Ca^{2+}	Mg^{2+}	F^-	Cl^-	NO_3^-	SO_4^{2-}	HCO_3^-	CO_3^{2-}	Si
								μmol L^{-1}										
Spring																		
HJ-1	2015/4/7	16.3	6.52	48.1	8.90	0.65	5.4	16	63	167	45	4	41	78	71	380	0	138
LQ-1	2015/4/7	16.3	7.68	221.3	10.96	1.50	1.8	44	147	989	103	4	135	257	117	1760	0	77
DR-1	2015/4/7	15.8	7.33	100.6	11.20	1.11	11.6	21	59	252	56	3	49	98	73	530	0	107
GL-1	2015/4/7	18.0	7.62	156.7	11.94	1.65	18.1	35	136	599	74	3	106	41	103	1200	0	107
CT-1	2015/4/7	17.5	8.26	222.6	11.42	1.59	1.7	22	51	926	168	2	60	89	96	1920	50	104
GY-1	2015/4/8	17.0	7.99	183.6	12.37	5.10	7.0	37	132	733	91	3	98	/	104	1520	0	89
XP-1	2015/4/8	18.5	8.04	182.9	11.54	0.95	4.4	35	118	716	98	5	93	82	105	1460	0	89
YL-1	2015/4/8	20.0	7.88	319.1	11.41	2.74	1.0	25	65	1334	364	4	84	34	102	3250	0	74
YS-1	2015/4/8	20.1	7.98	190.9	12.26	1.98	5.3	37	132	751	103	3	101	/	112	1610	0	97
Summer																		
HJ-2	2015/7/6	19.7	7.10	41.8	7.32	0.47	7.7	17	87	147	45	3	17	69	36	400	0	141
LQ-2	2015/7/6	22.1	7.56	186.6	7.29	0.60	4.3	32	67	877	73	2	89	203	111	1550	0	102
DR-2	2015/7/6	20.5	7.00	56.9	7.30	0.46	8.3	17	42	203	53	2	28	122	47	400	0	121
GL-2	2015/7/6	23.5	7.29	129.1	6.97	0.74	24.9	28	76	531	66	2	66	/	82	1000	0	139
CT-2	2015/7/6	21.7	7.88	180.6	7.50	0.73	25.8	21	32	795	147	2	39	/	72	1600	0	109
GY-2	2015/7/7	23.7	7.46	176.8	7.06	0.78	13.9	32	68	783	89	2	68	141	98	1500	0	108
XP-2	2015/7/7	23.1	7.70	166.0	6.96	1.12	11.6	29	64	733	87	3	62	/	93	1400	0	110
YL-2	2015/7/7	23.2	8.08	253.9	7.58	0.74	7.8	26	43	1139	271	2	59	22	75	2450	0	93
YS-2	2015/7/7	23.6	7.32	166.5	7.32	0.77	12.2	31	61	748	97	2	61	14	93	1500	0	106
Autumn																		
HJ-3	2015/10/18	23.0	8.16	48.8	9.66	0.53	13.5	14	81	154	46	5	17	66	54	360	10	89
LQ-3	2015/10/18	24.0	8.06	226.1	10.24	0.59	2.7	22	72	1069	97	2	66	124	113	1810	70	21
DR-3	2015/10/18	22.1	7.44	74.5	9.25	0.53	11.3	17	68	312	64	2	26	112	61	630	0	63
GL-3	2015/10/19	22.5	7.70	131.7	8.35	0.63	5.5	25	96	545	66	2	49	107	78	1010	0	52
CT-3	2015/10/18	22.0	7.89	203.5	9.86	0.72	4.4	18	51	894	178	2	33	93	88	1890	0	69
GY-3	2015/10/18	23.4	7.71	185.2	8.83	1.06	6.7	28	134	782	95	1	78	40	96	1540	0	50
XP-3	2015/10/17	24.5	8.05	182.8	10.17	0.68	4.0	29	126	799	96	3	70	/	101	1470	50	42
YL-3	2015/10/17	23.6	7.93	284.1	8.43	0.6	3.5	16	51	1216	307	2	44	146	74	2640	0	35
YS-3	2015/10/17	26.0	8.52	186.3	14.76	1.75	12.2	29	117	832	116	3	72	40	97	1490	100	66
Winter																		
HJ-4	2016/1/5	14.6	6.47	53.7	9.22	0.68	64.0	19	164	145	41	5	16	38	38	400	0	146
LQ-4	2016/1/5	16.3	7.40	245.1	9.15	0.46	5.3	37	91	1168	90	2	89	189	117	2050	0	52
DR-4	2016/1/5	14.4	6.45	53.8	9.65	0.35	20.2	17	60	224	47	2	21	88	40	400	0	119
GL-4	2016/1/5	16.8	7.00	263.5	11.64	0.53	13.0	39	303	1171	127	2	274	422	205	1600	0	169
CT-4	2016/1/5	16.8	7.82	206.4	11.26	0.94	2.1	17	42	909	157	2	32	89	68	1750	0	81
GY-4	2016/1/6	15.5	7.25	213.3	9.46	0.35	5.1	36	120	951	106	2	97	147	108	1550	0	85
XP-4	2016/1/6	15.9	7.46	227.5	10.16	0.38	3.2	35	118	1033	116	2	96	149	109	1900	0	82
YL-4	2016/1/7	16.7	7.74	348.3	9.70	0.33	10.3	21	55	1560	357	2	62	174	77	3300	0	69
YS-4	2016/1/7	15.8	7.31	238.0	9.72	0.46	19.8	33	114	1070	136	2	97	158	106	1950	0	84

"/" denotes below detection limit

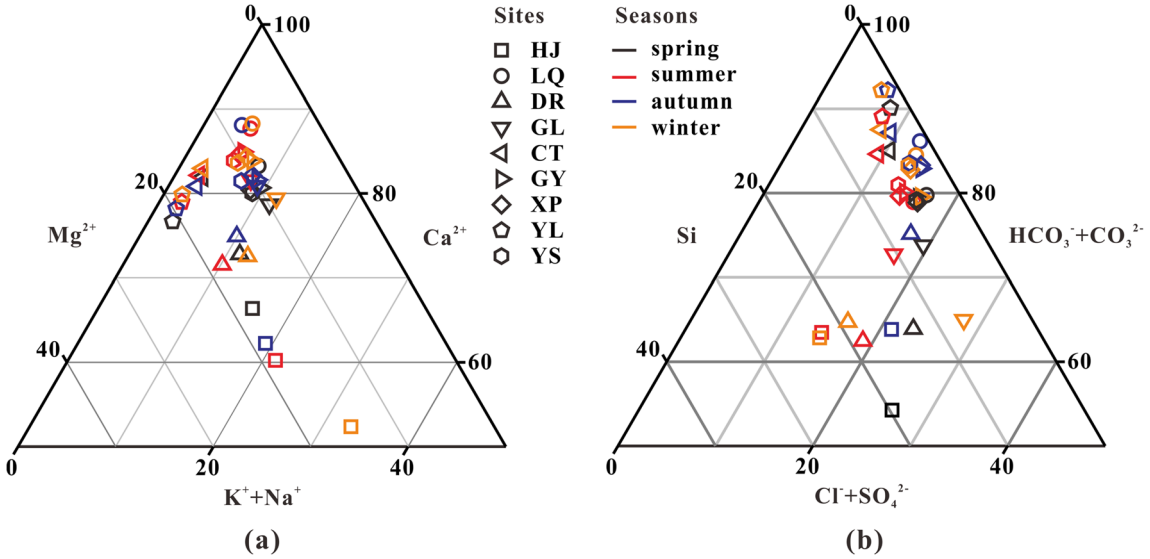

Fig. 2 Ternary diagrams showing the cation (**a**) and anion and Si (**b**) compositions of the river waters

Inorganic and OC concentrations and isotopes

DIC is composed of HCO_3^-, CO_3^{2-}, and dissolved CO_2. HCO_3^- was the dominant component in the study area, and CO_3^{2-} should not be ignored in waters with high pH values (Table 2). At sites HJ and DR, which mainly contained silicates, nearly half of the DIC was composed of dissolved CO_2, and the pH was approximately 6. The TSM, DOC, POC, ratio of POC and PON (POC/PON), and the carbon isotopes of DIC, DOC, and POC are presented in Table 3.

In the Lijiang River Basin, the DIC concentration was positivity correlated with the ratio of carbonate rock distribution area (Fig. 3b), varying between 0.38 and 3.45 mmol L^{-1}, with an average of 1.60 mmol L^{-1}. The average DIC concentrations in spring, summer, autumn, and winter were 1.61, 1.40, 1.52, and 1.90 mmol L^{-1}, respectively. Thus, the DIC concentration showed obvious seasonal variation and was higher in winter and lower in summer. $\delta^{13}C_{DIC}$ ranged from − 13.72 to − 8.83‰, and the April (spring), July (summer), October (autumn), and January (winter) averages were − 10.25‰, − 12.13‰, − 10.02‰, and − 10.54‰, respectively. The values were lower in summer and higher in spring and autumn.

The DOC concentration ranged from 0.03 to 0.45 mmol L^{-1}, with an average of 0.17 mmol L^{-1}. Similar to DIC, DOC was lower in summer. DOC was also positivity correlated with the ratio of carbonate rock distribution area (Fig. 3c). The $\delta^{13}C_{DOC}$ ranged from − 28.30 to − 21.46‰, with an average of − 25.96‰.

TSM varied from 1.59 to 54.90 mg L^{-1}, with an average of 2.06 mg L^{-1}, according to the variation in turbidity ($R = 0.87$). The POC concentration ranged from 0.01 to 0.25 mmol L^{-1}, with an average of 0.03 mmol L^{-1}. The POC concentration was positively correlated with TSM (Fig. 4a), and the contribution of POC to the TSM pool (%POC) ranged from 1.6 to 15.3%, with the highest values occurring when TSM was low (Fig. 4b). The POC/PON ratio ranged between 4.76 and 11.43, with an average of 7.39, was higher in summer (Fig. 4c) and increased with TSM (Fig. 4d). The $\delta^{13}C_{POC}$ ranges from − 28.21 to − 24.04‰ with an average of − 26.26‰ and is similar to the $\delta^{13}C_{DOC}$.

Discussion

Sources of major ions

The possible sources of major ion species in surface water are rock weathering, atmospheric precipitation, evaporation-crystallization, and anthropogenic inputs (Gibbs 1970). As shown in Fig. 2, the dominance of Ca^{2+} and HCO_3^- suggests that carbonate rock weathering dominates the water chemistry of the Lijiang River. According to the plots of the Ca^{2+}/Na^+ versus HCO_3^-/Na^+ and Ca^{2+}/Na^+ versus Mg^{2+}/Na^+ ratios (Fig. 5), the samples were located between carbonate rock and silicate rock weathering and according to the ratio of carbonate rock distribution area. For example, the samples from site HJ, which only had 2% carbonate rock, were located at the end-member of silicates (Fig. 5) due to the high abundance of Si and K^++Na^+ (Fig. 2). The samples from site YL, which had 90% carbonate rock, were located at the end-member of carbonates (Fig. 5).

As previously shown, Cl^-, which occurs in very low concentrations in rocks, is mainly from atmospheric inputs (Négrel et al. 1993; Roy et al. 1999). However, the K^+, Na^+, and Cl^- concentrations at sites LQ, GL, GY, XP, and YS, which were located near a city or town, were high, indicating that the inputs were from residential and industrial waters (Table 2). The Cl^-/Na^+ ratio ranged from 0.10 to 1.38, with

Table 3 Chemical composition and carbon isotopes of DIC, DOC, and POC in the Lijiang River Basin, Southwest China

Sample number	Date	TSM	DOC	POC	POC/PON	$\delta^{13}C_{DIC}$	$\delta^{13}C_{POC}$	$\delta^{13}C_{DOC}$
		mg L^{-1}				‰		
Spring								
HJ-1	2015/4/7	2.89	0.69	0.15	8.22	− 10.64	− 24.58	− 25.18
LQ-1	2015/4/7	1.80	2.71	0.08	7.39	− 10.67	− 26.49	− 21.46
DR-1	2015/4/7	8.52	1.40	0.30	7.99	− 11.23	− 26.68	− 25.72
GL-1	2015/4/7	15.30	2.62	0.73	7.86	− 9.03	− 25.89	− 25.90
CT-1	2015/4/7	2.91	2.86	0.19	7.63	− 10.83	− 26.32	− 26.61
GY-1	2015/4/8	5.77	2.61	0.34	7.40	− 9.35	− 26.52	− 25.47
XP-1	2015/4/8	5.45	2.39	0.23	7.61	− 9.43	− 26.01	− 25.42
YL-1	2015/4/8	2.16	4.08	0.12	6.80	− 11.30	− 27.73	− 26.04
YS-1	2015/4/8	3.98	2.73	0.13	7.31	− 9.78	− 24.04	− 26.72
Summer								
HJ-2	2015/7/6	7.49	1.57	0.28	11.43	− 13.72	− 28.21	− 25.40
LQ-2	2015/7/6	3.11	1.01	0.20	7.28	− 12.04	− 27.19	− 28.30
DR-2	2015/7/6	5.86	0.40	0.18	8.78	− 11.91	− 26.98	− 26.83
GL-2	2015/7/6	40.70	1.20	1.14	8.05	− 12.62	− 26.39	− 21.95
CT-2	2015/7/6	12.34	1.18	0.22	6.50	− 12.61	− 26.05	− 26.33
GY-2	2015/7/7	19.31	1.64	0.61	7.64	− 11.49	− 26.62	− 26.34
XP-2	2015/7/7	11.41	1.41	0.43	7.58	− 11.58	− 26.63	− 26.81
YL-2	2015/7/7	4.88	2.03	0.22	7.22	− 11.68	− 26.91	− 26.44
YS-2	2015/7/7	24.42	1.39	0.84	8.03	− 11.53	− 26.58	− 27.09
Autumn								
HJ-3	2015/10/18	18.71	0.71	0.43	7.84	/	− 24.17	− 25.89
LQ-3	2015/10/18	1.59	2.57	0.12	7.40	− 9.71	− 26.67	− 26.86
DR-3	2015/10/18	8.57	0.70	0.27	6.72	− 9.82	− 25.38	− 26.05
GL-3	2015/10/19	5.75	1.68	0.24	6.96	− 10.10	− 25.95	− 25.89
CT-3	2015/10/18	3.47	2.33	0.11	6.62	− 11.46	− 25.16	− 26.20
GY-3	2015/10/18	7.76	2.20	0.22	7.08	− 10.10	− 26.14	− 26.01
XP-3	2015/10/17	4.14	2.12	0.17	6.68	− 9.76	− 26.41	− 26.26
YL-3	2015/10/17	4.32	3.17	0.17	6.53	− 11.11	− 26.99	− 26.44
YS-3	2015/10/17	23.07	2.84	0.41	7.02	− 9.25	− 24.99	− 25.59
Winter								
HJ-4	2016/1/5	54.90	1.84	1.51	8.58	− 12.23	− 26.36	− 26.84
LQ-4	2016/1/5	2.06	2.89	0.18	7.27	− 10.48	− 26.96	− 26.85
DR-4	2016/1/5	14.49	0.72	0.24	7.50	− 10.94	− 26.47	− 25.31
GL-4	2016/1/5	19.64	5.39	3.01	4.76	− 9.54	− 24.48	− 24.93
CT-4	2016/1/5	2.30	1.70	0.18	6.57	− 10.70	− 26.31	− 26.18
GY-4	2016/1/6	4.37	2.40	0.22	7.05	− 9.49	− 26.87	− 26.24
XP-4	2016/1/6	3.31	2.28	0.17	7.09	− 10.07	− 26.96	− 26.16
YL-4	2016/1/7	1.83	2.63	0.09	6.38	− 11.06	− 27.06	− 26.39
YS-4	2016/1/7	35.17	2.64	0.46	7.09	− 10.35	− 26.01	− 25.57
Flood								
YS0-24	2015/5/9	105.54	3.15	2.77	/	/	− 25.40	/
YS08	2015/11/9	247.16	3.03	5.59	/	/	− 25.44	/

an average of 0.79, which was significantly lower than that of seawater (1.17, Berner and Berner 1987). The average Cl^-/Na^+ ratio at site YL, which was mainly covered by carbonates (90%), was 1.16, similar to the ratio of seawater. For the sites covered mainly by silicates, i.e., sites HJ and DR, the average Cl^-/Na^+ ratios were 0.29 and 0.56, respectively. The

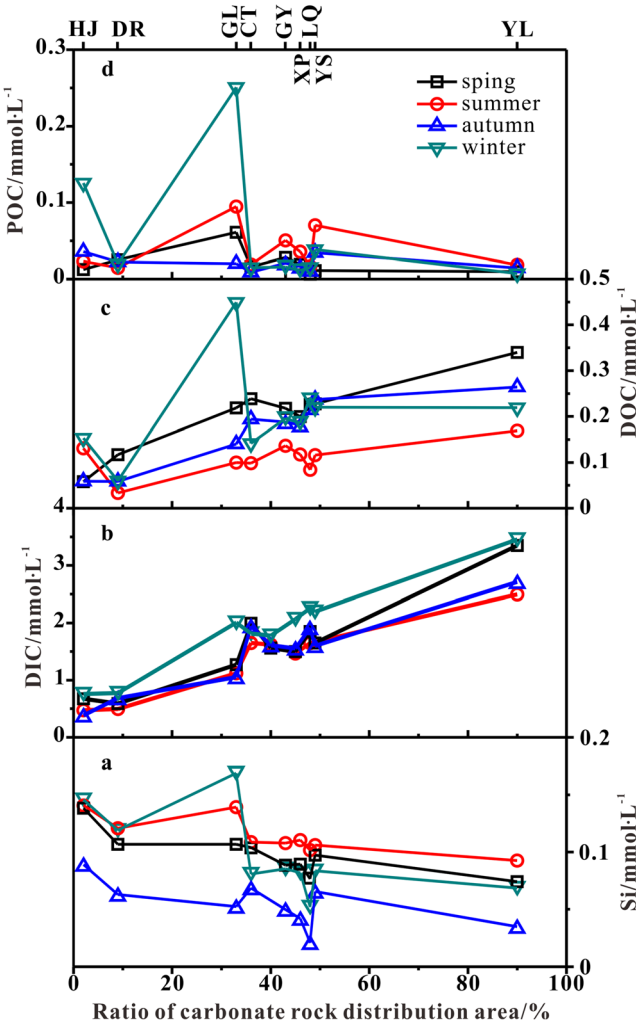

Fig. 3 Distributions of the Si, DIC, DOC, and POC concentrations in different locations and seasons

concentration of excess Na^+ can be calculated as $[Na^+]$-$[Cl^-]$/1.17. The average of excess Na^+ in the sites was positivity correlated with the ratio of silicate rock distribution area (R = 0.71). Thus, silicate rock weathering was the main source of excess Na^+ to Cl^-.

The SO_4^{2-} concentrations of precipitation in Guilin ranged from 28.54 to 375.00 μmol L^{-1} with the average of 87.32 μmol L^{-1}, and the NO_3^- concentrations ranged from 20.32 to 225.81 μmol L^{-1} with the average of 60.13 μmol L^{-1} (Zhang et al. 2012b). Both of them mainly originated from anthropogenic sources (Guo et al. 2016). The SO_4^{2-} and NO_3^- concentrations of samples were higher than those of precipitation, with averages of 89 and 95 μmol L^{-1}, respectively. The SO_4^{2-} concentration of the water was similar to that of the precipitation, and the coefficient of variation was small. Forests and scattered villages dominate the HJ and DR river basins (Table 2), and the contribution of local human activities to the SO_4^{2-} concentration of precipitation was low. As a result, the SO_4^{2-} concentrations at sites HJ and DR were also lower (Table 2). The SO_4^{2-} concentration and SO_4^{2-}/Cl^- ratio of precipitation were 7~933 μmol L^{-1} and 0.54~11.60, respectively (data from the Guilin Environmental Protection Bureau). The SO_4^{2-} concentration and SO_4^{2-}/Cl^- ratio of the samples were 36~205 and 0.75~3.20, respectively, which were within the range of the precipitation values. There was little sulfur in the strata, and therefore, the SO_4^{2-} concentration in the water must have originated from precipitation. The reaction between anthropogenic SO_2 from coal combustion and automobile exhaust in the atmosphere and free radicals of OH and/or aqueous H_2O_2 in droplets is the main source of H_2SO_4 (Berner and Berner 1987). The SO_4^{2-} in the river water indicated that the reaction between carbonate rocks and sulfuric acid from precipitation was the source (Li et al. 2008). The NO_3^- concentration in the water was much higher than that of precipitation, and therefore, NO_3^- was sourced from precipitation and the nitrification of N fertilizers in soil (Gandois et al. 2011). As shown in Table 2, the NO_3^- concentrations in some samples were below the detection limit because of uptake by aquatic phototrophs. Because of pollutant discharge from Guilin city, the SO_4^{2-} and NO_3^- concentrations were especially high in the GL-4 sample (Table 2). As discussed above, sulfuric acid sourced from precipitation and nitric acid derived from precipitation and nitrification are common in this area. Except for sites HJ and DR, the $[Ca^{2+}+Mg^{2+}]/[HCO_3^- + CO_3^{2-}]$ equivalent ratios ranged from 1.05 to 1.62, and the $[Ca^{2+}+Mg^{2+}]/[HCO_3^- + CO_3^{2-} + SO_4^{2-} + NO_3^-]$ equivalent ratios ranged from 0.93 to 1.10, with an average of 1.00. This result indicates carbonate rock weathering by both carbonic acid and sulfuric/nitric acid (Martin 2017). The equivalent ratios of $[Ca^{2+}+Mg^{2+}]/[HCO_3^- + CO_3^{2-} + SO_4^{2-} + NO_3^-]$ ranged from 0.70 to 0.87 at sites HJ and DR, which were dominated by silicate rocks. Based solely on carbonate weathering, ions are not balanced. Silicate weathering contributes relatively more to water chemistry, and the K^+ and Na^+ derived from silicate weathering should participate in the balance.

Si is mainly derived from silicate weathering (Turner and Rabalais 1991) and is sensitive to many biogeochemical processes, such as reservoir retention, plant uptake, and the secondary Si-bearing phase (Humborg et al. 1997; Maher and Chamberlain 2014; Torres et al. 2015). As shown in Fig. 3a, the concentrations of Si decreased with decreasing ratios of silicate rock distribution area (subtract the ratio of carbonate rock distribution area from 100%). Therefore, Si was mainly derived from silicate weathering. At site LQ, the river is shallow, and aquatic phototrophs flourish. Si can be used by aquatic phototrophs in this situation. Thus, the Si concentration at site LQ was obviously lower than those at sites XP and YS, which had silicate rock distribution areas that were similar to that at the LQ site (Fig. 3a). Because of pollutant discharge from Guilin city, the Si concentration was especially high in the GL-4 sample (Fig. 3a).

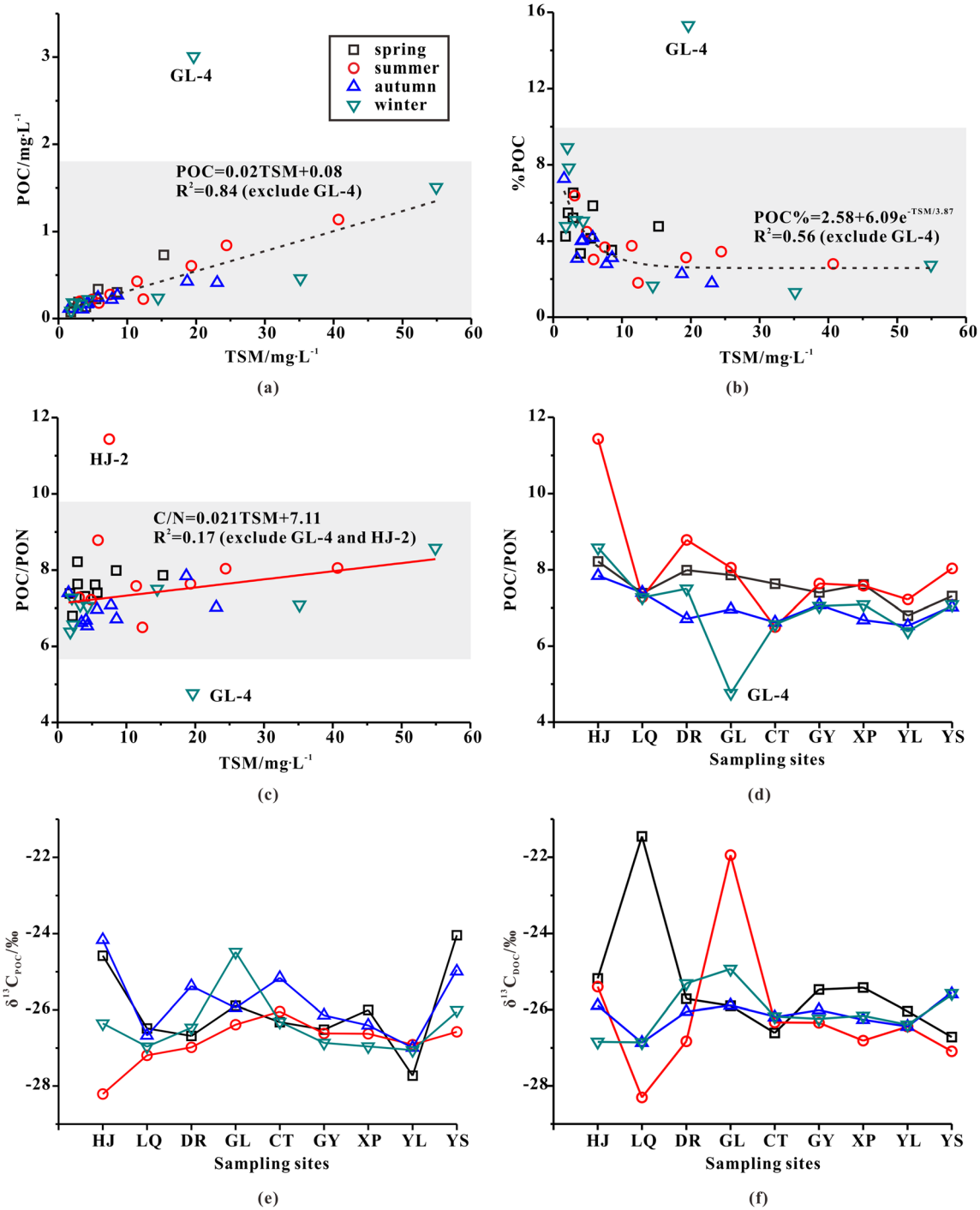

Fig. 4 Cross plots showing TSM vs. POC, POC%, and POC/PON (**a**–**c**); distributions of POC/PON, $\delta^{13}C_{POC,}$ and $\delta^{13}C_{DOC}$ in different sites and seasons (**d**–**f**)

Source of DIC based on chemical weathering

As discussed above, the chemical weathering of carbonates and silicates is the main source of DIC in the study area. The reactions are shown in the equations below.

Carbonate weathering ($0 \le x \le 1$):

$$Ca_xMg_{1-x}CO_3 + CO_2 + H_2O \rightarrow xCa^{2+} + (1-x)Mg^{2+} + 2HCO_3^- \quad (1)$$

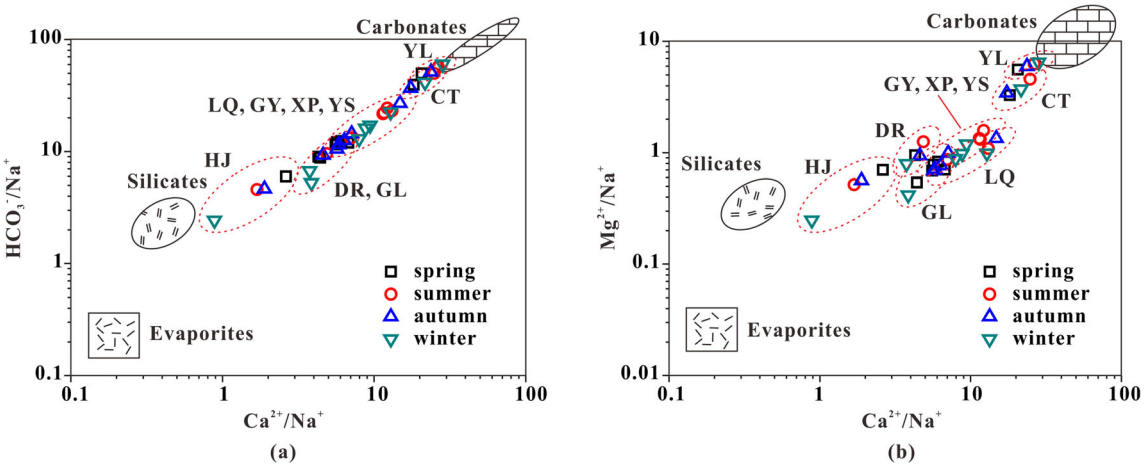

Fig. 5 Plots of the Ca^{2+}/Na^{+} versus Mg^{2+}/Na^{+} and Ca^{2+}/Na^{+} versus HCO_3^{-}/Na^{+} ratios of the river waters

$$2Ca_xMg_{1-x}\,CO_3 + H_2SO_4 \rightarrow 2xCa^{2+} + 2(1-x)Mg^{2+} + 2HCO_3^{-} + SO_4^{2-} \quad (2)$$

$$Ca_xMg_{1-x}\,CO_3 + HNO_3 \rightarrow xCa^{2+} + (1-x)Mg^{2+} + HCO_3^{-} + NO_3^{-} \quad (3)$$

Silicate weathering ($0 \le x \le 1$):

$$Ca_xMg_{1-x}Al_2Si_2O_8 + 2H_2CO_3 + 6H_2O \rightarrow xCa^{2+} + (1-x)Mg^{2+} + 2HCO_3^{-} + 2H_4SiO_4 + 2Al(OH)_3 \quad (4)$$

$$Na_xK_{1-x}AlSi_3O_8 + H_2CO_3 + 5H_2O \rightarrow xNa^{+} + (1-x)K^{+} + HCO_3^{-} + 3H_4SiO_4 + Al(OH)_3 \quad (5)$$

Accordingly:

$$HCO_3 = HCO_3\_sil + HCO_3\_carb\_car + HCO_3\_carb\_s/n \quad (6)$$

$$Ca = Ca\_sil + Ca\_carb\_car + Ca\_carb\_s/n \quad (7)$$

$$Mg = Mg\_sil + Mg\_carb\_car + Mg\_carb\_s/n \quad (8)$$

$$HCO_3\_carb\_car = 2(Ca\_carb\_car + Mg\_carb\_car) \quad (9)$$

$$HCO_3\_carb\_s/n = Ca\_carb\_s/n + Mg\_carb\_s/n \quad (10)$$

The subscripts carb and sil denote carbonate and silicate origins, respectively. HCO_3_sil represents bicarbonate from silicate weathering. HCO_3_carb_car and HCO_3_carb_s/n denote bicarbonate sourced from reactions of carbonate with carbonic acids and sulfuric/nitric acids, respectively. The subscripts for Ca and Mg are the same as those for HCO_3.

In previous studies, HCO_3_sil was calculated based on the Na^{+} and K^{+} concentrations (Han and Liu 2004; Xu and Liu 2007; Sun et al. 2010). Those calculations were based on the hypothesis that all sodium and potassium are derived from silicate weathering after subtracting the chloride origin. However, the K^{+}+Na^{+}-Cl^{-} concentrations at sites GL, GY, XP, and YS, which were located near a city or town, were high; thus, the sodium and potassium concentrations in the samples reflected the influence of anthropogenic activity in the study area. As mentioned above, the Si concentration had a good correction with the proportion of silicate rock. Therefore, HCO_3_sil was calculated with the Si concentration in this study.

The (Ca + Mg)/(K + Na) ratio for the silicate fraction should be 0.6 in the study area because the rivers drain purely silicate terrains in the Pearl River (Zhang et al. 2007). Thus, the equations for silicate weathering based on Eqs. (4) and (5) are below:

$$\begin{aligned} &0.6(Ca_xMg_{1-x}Al_2Si_2O_8 + 2H_2CO_3 + 6H_2O) \\ &+ (Na_xK_{1-x}AlSi_3O_8 + H_2CO_3 + 5H_2O) \rightarrow \\ &0.6\left(xCa^{2+} + (1-x)Mg^{2+} + 2HCO_3^{-} + 2H_4SiO_4 + 2Al(OH)_3\right) \\ &+ \left(xNa^{+} + (1-x)K^{+} + HCO_3^{-} + 3H_4SiO_4 + Al(OH)_3\right) \end{aligned} \quad (11)$$

$$HCO_3\_sil = 0.52 \times Si \quad (12)$$

$$Ca\_sil + Mg\_sil = 0.14 \times Si \quad (13)$$

For equation (14), the CO_3^{2-} was assumed to be HCO_3^{-}, with twice the concentration in the calculation.

$$2HCO_3^{-} = CO_3^{2-} + CO_2 + H_2O \quad (14)$$

Based on Eqs. (6) to (13), the sources of DIC were calculated. As shown in Fig. 6, carbonate weathering by carbonic acid was the dominant source of bicarbonate, ranging from 29.7 to 93.7%, with an average of 75.1%. The contribution of carbonate weathering by sulfuric/nitric acid ranged from 1.6 to 64.8%, with an average of 19.6%. The contributions were high in summer and winter for the inputs of sulfuric and nitric acids by runoff and human activities (Fig. 6). Spatially, these contributions were high at sites GL, DR, and LQ, which were influenced by Guilin city and Xing'an town, and low at

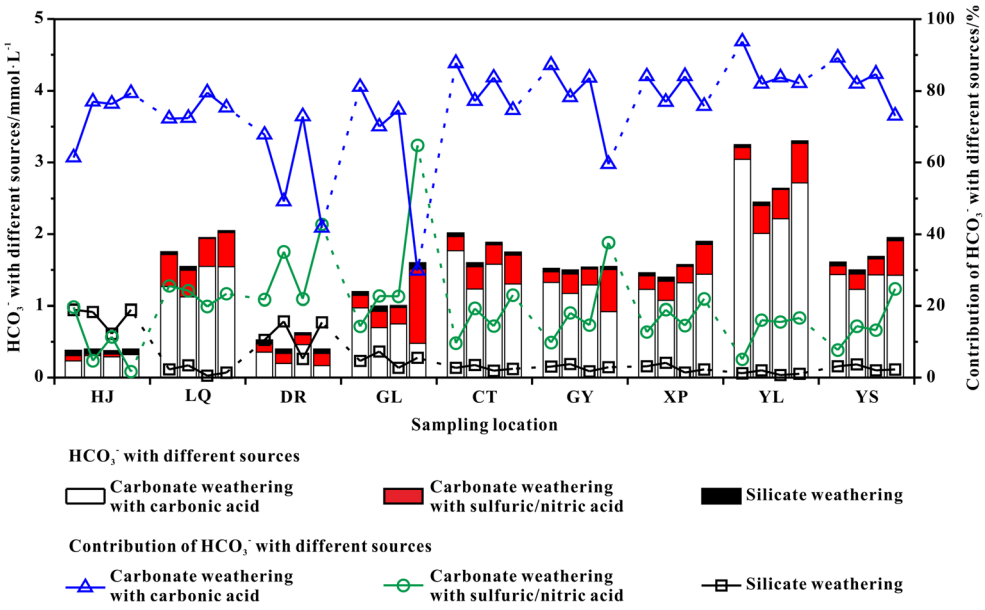

Fig. 6 Sources of bicarbonate in different locations and seasons. The four samples from spring to winter in each sampling location were arranged from left to right

sites HJ and YL, which were mostly covered by vegetation. The contribution of silicate weathering was highest at site HJ and lowest at site YS (Fig. 6) according to the ratio of silicate distribution area.

$\delta^{13}C_{DIC}$ variation and aquatic phototrophs

As shown in Table 2, the average pH values in spring and autumn were higher than those in summer and winter; chlorophyll was highest in spring, followed by autumn, summer, and winter; and DO was highest in spring, followed by winter, autumn, and summer. Previous studies have shown that bicarbonate can be used by aquatic phototrophs in karst areas (Liu et al. 2010; Wang et al. 2013; Pu et al. 2017). When bicarbonate is taken up by aquatic phototrophs, the pH value and DO both increase (Zhang et al. 2012a; Chen et al. 2014b; Pu et al. 2019). Chlorophyll is a major parameter that explains the primary products in rivers (Yang et al. 2016). Chlorophyll, DO, and pH were high in spring and autumn, and as a result, bicarbonate uptake by aquatic phototrophs was significant in spring and autumn.

The possible processes other than rock weathering that may influence $\delta^{13}C_{DIC}$ include (1) carbonate precipitation; (2) exchange with atmospheric CO_2; (3) CO_2 directly coming from soil; and (4) river photosynthesis and respiration (Sun et al. 2015). The theoretical $\delta^{13}C_{DIC}$ value of rock weathering can be calculated by the contributions of different sources.

$$\delta^{13}C_{DIC\_Th} = a_{sil}\delta^{13}C_{sil} + a_{carb\_car}\delta^{13}C_{carb\_car} + a_{carb\_s/n}\delta^{13}C_{carb\_s/n} \quad (15)$$

$$a_{sil} + a_{carb\_car} + a_{carb\_s/n} = 1 \quad (16)$$

In the equation, $\delta^{13}C_{DIC\_Th}$ denotes the theoretical $\delta^{13}C_{DIC}$ value based on the chemical weathering of silicates and carbonates; a_{sil}, a_{carb_car}, and $a_{carb\_s/n}$ denote the contributions of silicate weathering and carbonate weathering by carbonic acid and sulfuric/nitric acid, respectively, which were calculated above; and $\delta^{13}C_{sil}$, $\delta^{13}C_{carb\_car}$, and $\delta^{13}C_{carb\_s/n}$ denote the theoretical $\delta^{13}C$ values of silicate weathering and carbonate weathering by carbonic acid and sulfuric/nitric acid, respectively.

As shown in Eqs. (1) to (5), HCO_3^- from silicate weathering is only derived from atmospheric/soil CO_2; HCO_3^- from carbonate weathering by sulfuric/nitric acid is only derived from carbonates; and half of the HCO_3^- from carbonate weathering by carbonic acid is derived from atmospheric/soil CO_2, and half is derived from carbonates. Carbonates in the Lijiang River Basin are marine carbonates, and the carbon isotopes range from − 4.40 to 2.90‰, with an average of 0‰ (Peng and Hu 2001); thus, $\delta^{13}C_{carb\_sulf}$ is 0‰ in the study area. The concentration of soil CO_2 is many times higher than the atmospheric CO_2 concentration (Cao et al. 2011), and therefore, $\delta^{13}C_{sil}$ and $\delta^{13}C_{carb\_car}$ depend on the carbon isotope of soil CO_2 ($\delta^{13}C_{soil}$). The $\delta^{13}C_{soil}$ value in the Lijiang River Basin ranges from − 29.35 to − 18.26‰, with an average of − 24.26‰ (Cao et al. 2011); the $\delta^{13}C_{DIC}$ value of karst springs and subterranean streams in the Lijiang River Basin range from − 9.24 to − 15.03‰, with an average of − 12.34‰ (Huang et al. 2015), nearly half of the $\delta^{13}C_{soil}$ value mentioned above. However, the samples were also influenced by sulfuric/nitric acid (Eqs. (2) and (3)), and therefore, the $\delta^{13}C_{DIC}$ value from carbonate weathering by

carbonic acid was lower than − 12.34‰, and the average $\delta^{13}C_{soil}$ should be lower than − 24.68‰. Because of carbon isotope fractionation, the carbon isotope of dissolved CO_2 is approximately − 1.3‰ lighter than that of gaseous CO_2 (Zhang et al. 1995). Therefore, − 25.5‰ can be used for $\delta^{13}C_{soil}$ in the study area, and $\delta^{13}C_{sil}$ and $\delta^{13}C_{carb\_car}$ were − 25.5‰ and − 12.75‰, respectively.

As shown in Fig. 7, the $\delta^{13}C_{DIC}$ values of the samples in spring and autumn were higher than $\delta^{13}C_{DIC\_Th}$ ($\delta^{13}C_{DIC}$-$\delta^{13}C_{DIC\_Th} > 0$). As previously discussed, bicarbonate uptake by aquatic phototrophs is significant in spring and autumn. In the process of aquatic phototrophs photosynthetic uptake of bicarbonate, aquatic phototrophs preferentially consume ^{12}C during photosynthesis, leading to a simultaneous decrease in DIC concentration and increase in $\delta^{13}C_{DIC}$ of river water (Zhang et al. 2012a; Chen et al. 2014b). The $\delta^{13}C_{DIC}$ values of the samples in summer and winter were lower than $\delta^{13}C_{DIC\_Th}$ (Fig. 7). It was rainy before the summer and winter sampling, and the turbidity and TSM were high (Tables 1 and 2); therefore, the photosynthesis of aquatic phototrophs was weak, and $\delta^{13}C_{DIC}$ fractionation influenced by aquatic phototrophs was not significant. Additionally, more soil CO_2 with a low $\delta^{13}C_{DIC}$ value was taken by runoff and participated in carbonate weathering, and therefore, the $\delta^{13}C_{DIC}$ value was lower. As shown in Fig. 7, in spring and autumn, the relatively higher $\delta^{13}C_{DIC}$ to $\delta^{13}C_{DIC\_Th}$ was more remarkable in the mainstream from Guilin to Yangshuo, where the river is wide, the water is shallow, and aquatic phototrophs thrive. The concentration of bicarbonate was also high in this mainstream (Fig. 3). High DIC, low water flow, and low TSM provide a sufficient carbon source and suitable environment for bicarbonate uptake by aquatic phototrophs photosynthesis and result in high $\delta^{13}C_{DIC}$ values.

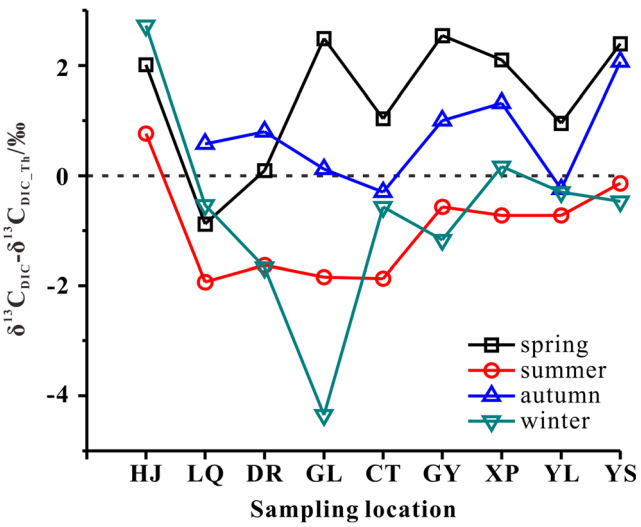

Fig. 7 Distribution of the difference between $\delta^{13}C_{DIC}$ and $\delta^{13}C_{DIC\_Th}$ ($\delta^{13}C_{DIC}$-$\delta^{13}C_{DIC\_Th}$)

Origin of POC and DOC

As shown in Fig. 4, there was striking covariation between %POC and TSM, which has been noted in previous studies (Tao et al. 2004; Bouillon et al. 2012). Two mechanisms have been invoked to explain this relationship: (a) a higher contribution by in situ production (i.e., phytoplankton with a high %POC) during periods of low turbidity, and (b) a gradient of contributions by direct litter inputs or topsoil (with a relatively higher %POC) and deeper soil layers with a lower %POC during high runoff events (Bouillon et al. 2012). For the Lijiang River, we propose that a high phytoplankton contribution is the main cause of the covariation between %POC and TSM.

As previously discussed, DIC uptake by aquatic phototrophs is significant in spring and autumn because of low turbidity and contributes more to POC. The average POC/PON ratios were 7.58, 6.98, and 6.92 in spring, autumn, and winter, respectively. The C/N ratio of phytoplankton is 6.6 (Redfield 1958; LaZerte 1983; Huang et al. 2018), and therefore, these low POC/PON ratios match those that would be expected when phytoplankton are predominant. The average POC/PON ratio was 8.06 in summer, higher than those in the other seasons, and therefore, soil OC contributed more to POC. The average C/N ratios of soils are 14.6 and 14.3 in karst and nonkarst areas, respectively, in the Lijiang River Basin (Cao et al. 2011). The C/N ratios of sediments in Huixian wetland, which is a typical karst wetland in the Lijiang River Basin, decreased from 20.4 to 9.0 from the bottom to the top, indicating the contribution of aquatic phototrophs to sediment organic matter increases (Zhou 2015). This result has also been proven by sporopollen studies (Zhou 2015). Sediment organic matter is dominated by allochthonous inputs when the C/N ratio is higher than 15 (Zhou 2015). Therefore, we propose a C/N ratio of 15 for the end of allochthonous inputs and 6.6 for the end of autochthonous inputs. The contribution of autochthonous inputs to POC ranged from 42 to 100%, with an average of 82%, based on the calculation of POC/PON. The POC/PON ratio of sample GL-4 was 4.76, and the %POC was especially higher than those of the other samples, indicating direct litter inputs, which coincides with the chemical characteristics discussed above.

Similar to POC, DOC in the Lijiang River is impacted by rock weathering, photosynthetic activity, and fluvial erosion. DOC increased with DIC and showed a positive correlation with DIC (R = 0.68). The concentrations of DOC and POC both increased during floods, but the DOC/POC ratio decreased, ranging from 0.24 to 1.00, with an average of 0.44 (Sun et al. 2007). During high runoff events, both POC and DOC are sourced relatively more from allochthonous inputs during floods. However, in the study area, DOC was lower in summer when the discharge was higher; moreover, POC was

also higher (Fig. 3). The DOC/POC ratio ranged from 1.05 to 35.42 and showed a positive correlation with DIC ($R = 0.71$). Therefore, we propose that autochthonous organic sources in the Lijiang River were the dominant input to DOC when flooding was not occurring. Lipid biomarkers are extensively used to distinguish autochthonous and allochthonous sources; during sampling of the Pearl River from January to February 2015, which included three samples from the Lijiang River, more than 65% of riverine organic matter was sourced from autochthonous inputs (Yang et al. 2016). This result was similar to the POC results discussed above.

POC and DOC were both mainly sourced from the process of in-river primary production in this study. The ratio of autochthonous OC increased with TSM when the TSM concentration was low (TSM < 150 mg L^{-1}) and decreased with the TSM when the TSM concentration was high (TSM > 150 mg L^{-1}) (Yang et al. 2016). The TSM concentrations of the samples in this study were all lower than 55 mg L^{-1} (Table 3) and were beneficial for photosynthetic activity. Therefore, DIC is taken up by aquatic phototrophs and converted into OC in the Lijiang River.

Evaluation of bicarbonate-transformed OC in riverine OC

In the previous discussion, autochthonous OC was dominant in Lijiang River OC when TSM was low. During photosynthesis, aquatic phototrophs first uptake carbon dioxide in air and water as the carbon source, and in-river bicarbonate can also participate in photosynthesis under the action of carbonic anhydrase (Mcconnaughey 1998; Li et al. 2011a; Lian et al. 2011). The protons needed for bicarbonate-based photosynthesis are derived largely from calcification (Mcconnaughey 1998). Thus, photosynthesis is a reaction with calcification, and the pH value, DO, and $CaCO_3$ saturation increase, as shown above.

$$Ca^{2+} + 2HCO_3^- \rightarrow CaCO_3 + CH_2O + O_2 \quad (17)$$

The carbon isotopes of OC can be used to distinguish between autochthonous and allochthonous sources (Waterson and Canuel 2008; Huang et al. 2018), but it must be combined with the C/N in the karst area. Allochthonous OC is mainly sourced from soil. C3 plants, with carbon isotopes ranging from − 34 to − 22‰ (Boutton et al. 1994), are dominant; thus, the carbon isotopes of soil OC ranged from − 28 to − 19‰ in the Pearl River Basin (Pan et al. 2002; Chen et al. 2005; Sun et al. 2015). The carbon isotopes for aquatic phototrophs in the Lijiang River also ranged from − 30 to − 19‰ (Zhang et al. 2013). Therefore, the isotope of autochthonous OC was similar to that of allochthonous OC.

The carbon isotopes for aquatic phototrophs differ in different karst areas because carbon sources and DIC utilization strategies are the dominant influencing factors (Wu et al. 2012; Li et al. 2015). The carbon isotopes became obviously heavier only 500 m from upstream to downstream in a karst area because the HCO_3^-/CO_2 ratio increased (Wang et al. 2017). The CO_2 concentration was high in a debouchure, and aquatic phototrophs mainly used CO_2 (Clement et al. 2016, 2017). The CO_2 concentration decreased rapidly downstream, and the aquatic phototrophs mainly used bicarbonate at low CO_2 concentrations with the participation of carbonic anhydrase (Clement et al. 2016, 2017). Therefore, the carbon isotopes of autochthonous sources varied in the Lijiang River and depended on the proportions of carbon dioxide- and bicarbonate-based photosynthesis. Autochthonous OC can be divided into two end-members that are totally sourced from bicarbonate or carbon dioxide.

As discussed above, there are three sources of river OC: allochthonous OC, autochthonous OC sourced from bicarbonate, and autochthonous OC sourced from carbon dioxide. Therefore, the carbon isotopes of OC alone cannot distinguish these three sources, and these data should be combined with the POC/PON ratio, as discussed above, which can distinguish allochthonous OC and autochthonous OC. The $\delta^{13}C_{POC}$ value during two flood events was − 25.42‰ (Table 3), which can be used as the average carbon isotope value of allochthonous inputs in the study area. In previous studies, the carbon isotopes of autochthonous inputs sourced from bicarbonate and carbon dioxide were − 22.74‰ and − 31.56‰, respectively (Wu et al. 2011; Zhang et al. 2013; Li et al. 2015). Therefore, these three sources can be quantitatively estimated by considering their $\delta^{13}C$ values and POC/PON ratios as end-members (Fig. 8):

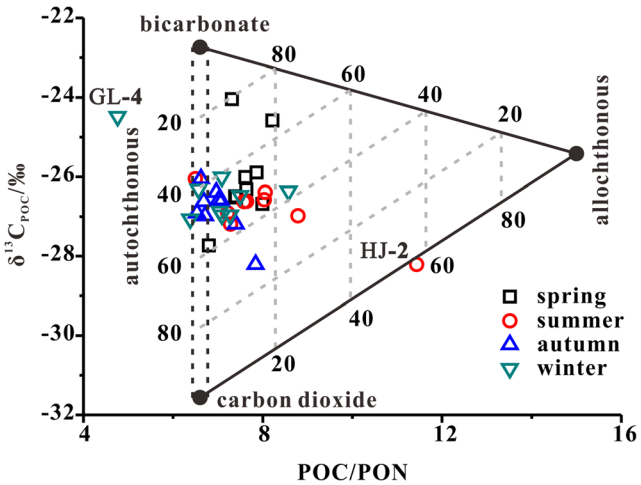

Fig. 8 Plots of POC/PON versus $\delta^{13}C_{POC}$ in different locations and seasons

$$\delta^{13}C_{POC} = \delta^{13}C_{al} * f_{al} + \delta^{13}C_{au\_B} * f_{au\_B} + \delta^{13}C_{au\_C} * f_{au\_C} \quad (18)$$

$$f_{au} = f_{au\_B} + f_{au\_C} \quad (19)$$

In the equations, $\delta^{13}C_{POC}$, $\delta^{13}C_{al}$, $\delta^{13}C_{au\_B}$, $\delta^{13}C_{au\_C}$ are the $\delta^{13}C$ values of the bulk sample, allochthonous inputs, and autochthonous inputs sourced from bicarbonate and carbon dioxide, respectively; and f_{al}, f_{au_B}, and f_{au_C} are the fractional abundances of each of the three sources, respectively. Based on the POC/PON ratio, f_{al} and f_{au} are the contributions of allochthonous and autochthonous inputs, as calculated above. $\delta^{13}C_{al}$ was − 25.42‰ based on the $\delta^{13}C_{POC}$ value during floods. In previous studies, $\delta^{13}C_{au\_B}$ and $\delta^{13}C_{au\_C}$ were − 22.74‰ and − 31.56‰, respectively (Wu et al. 2011; Zhang et al. 2013; Li et al. 2015), and could be used in the Lijiang River because of the similar variation in aquatic phototrophs carbon isotopes.

The results showed that the percentage contribution of in-river primary production with bicarbonate-based photosynthesis to POC ranged from 33.8 to 79.4%, with an average of 54.0%, except for samples HJ-2 and GL-4 (Fig. 8). The percentages of bicarbonate-transformed OC were different in different seasons, higher in spring (54.6%) and autumn (62.5%) and lower in summer (46.8%) and winter (50.8%). The average carbon isotope of DOC was similar to that of POC, and therefore, the contribution of in-river primary production with bicarbonate-based photosynthesis was also the main source for DOC.

As discussed above, nearly half of the riverine OC was bicarbonate-transformed OC. The average riverine OC was approximately 17% of the DIC; thus, approximately 8% of the bicarbonate was transformed into OC by aquatic phototroph photosynthesis.

Conclusions

This study focused on seasonal hydrochemical, inorganic, and OC variations in a typical karst basin. As the study basin was a karst basin, the DIC was mainly derived from the weathering of carbonates and was positively correlated with the ratio of carbonates. The weathering of carbonates by sulfuric and nitric acids was stronger in summer and winter when human activity was more intense.

The water chemistry was also obviously influenced by aquatic phototrophs, which led to increases in pH and DO and heavier $\delta^{13}C_{DIC}$. This result was related to the process of bicarbonate transformation to OC by aquatic phototrophs. This process was more remarkable in spring and winter and in the mainstream from Guilin to Yangshuo, which benefited the growth of aquatic phototrophs.

The riverine OC inputs were mainly autochthonous, and more than half of the autochthonous carbon was sourced from bicarbonate uptake by aquatic phototrophs. Therefore, DIC, which is mainly derived from the weathering of carbonates, was transformed to riverine OC. This OC was nearly half of the total OC and 8% of DIC in the typical karst basin.

Funding information This study was financially supported by the National Natural Science Foundation of China (Grant Nos. 41402238, 41402324), the Project of Natural Science Foundation of Guangxi (Grant Nos. 2016GXNSFBA380174, 2017GXNSFFA198006), the Project of Institute of Karst Geology, CAGS (2016001), and the Project of the China Geological Survey (DD20190022).

References

Berner EK, Berner RA (1987) The global water cycle: geochemistry and environment, vol 394. Prentice-Hall, New York

Bouillon S, Yambélé A, Spencer RGM, Gillikin DP, Hernes PJ, Six J, Merckx R, Borges AV (2012) Organic matter sources, fluxes and greenhouse gas exchange in the Oubangui River (Congo River basin). Biogeosciences 9:2045–2062

Boutton TW, Archer SR, Nordt LC (1994) Climate, CO_2 and plant abundance. Nature 372:625–626

Cao J, Zhou L, Yang H, Lu Q, Kang Z (2011) Comparison of carbon transfer between forest soils in karst and clasolite areas and the karst carbon sink effect in Maocun village of Guilin. Quat Sci 31:431–437

Chen Q, Shen C, Sun Y, Peng S, Yi W, Li Z, Jiang M (2005) Spatial and temporal distribution of carbon isotopes in soil organic matter at the Dinghushan Biosphere Reserve, South China. Plant Soil 273:115–128

Chen B, Li W, Chen Q, Liu D (2014a) Effects of different bottom sediment and submerged macrophytes on macrofauna communites in the Lijiang River during the summer. Acta Sci Circumst 34:1758–1765

Chen B, Yang R, Liu Z, Yan H, Zhao M (2014b) Effects of aquatic phototrophs on diurnal hydrochemical and $\delta^{13}C_{DIC}$ variations in an epikarst spring and two spring-fed ponds of Laqiao, Maolan, SW China. Geochimica 43:375–385

Ciais P et al (2013) Carbon and other biogeochemical cycles. In: Stocker TF et al (eds) Climate Change 2013: The physical science basis. Contribution of Working Group I to the Fifth Assessment Report of the Intergovernmental Panel on Climate Change. Cambridge University Press, Cambrige and New York, pp 465–570

Clement R, Dimnet L, Maberly SC, Gontero B (2016) The nature of the CO_2-concentrating mechanisms in a marine diatom, Thalassiosira pseudonana. New Phytol 209:1417–1427

Clement R, Jensen E, Prioretti L, Maberly SC, Gontero B (2017) Diversity of CO_2-concentrating mechanisms and responses to CO_2 concentration in marine and freshwater diatoms. J Exp Bot 68:3925–3935

Gaillardet J, Dupré B, Louvat P, Allègre CJ (1999) Global silicate weathering and CO_2 consumption rates deduced from the chemistry of large rivers. Chem Geol 159:3–30

Gandois L, Perrin AS, Probst A (2011) Impact of nitrogenous fertilizer-induced proton release on cultivated soils with contrasting carbonate contents: a column experiment. Geochim Cosmochim Acta 75:1185–1198

Gibbs RJ (1970) Mechanisms Controlling World Water Chemistry. Science 170:1088–1090

Guo Y, Yu S, Li Y, Sun P, He R (2016) Chemical characteristics and source of acid precipitation in Guilin. Environ Sci 37:2897–2905

Han G, Liu C (2004) Water geochemistry controlled by carbonate dissolution: a study of the river waters draining karst-dominated terrain, Guizhou Province, China. Chem Geol 204:1–21

Hindshaw RS, Tipper ET, Reynolds BC, Lemarchand E, Wiederhold JG, Magnusson J, Bernasconi SM, Kretzschmar R, Bourdon B (2011) Hydrological control of stream water chemistry in a glacial catchment (Damma Glacier,Switzerland). Chem Geol 285:215–230

Huang Q, Qin X, Liu P, Tang P (2015) Impact of acid rain to $\delta^{13}C_{DIC}$ of karst groundwater and carbon sink in dry season in Guilin. Earth Sci (J China Univ Geosci) 40:1237–1247

Huang S, Pu J, Cao J, Li J, Zhang T, Jiang F, Li L, Wu F, Pan M, Bai B (2018) Origin and effect factors of sedimentary organic carbon in a karst groundwater-fed reservoir, South China. Environ Sci Pollut Res 25:8497–8511

Humborg C, Ittekkot V, Cociasu A, Bodungen BV (1997) Effect of Danube River dam on Black Sea biogeochemistry and ecosystem structure. Nature 386:385–388

Lang SQ, Bernasconi SM, Früh-Green GL (2012) Stable isotope analysis of organic carbon in small (μg C) samples and dissolved organic matter using a GasBench preparation device. Rapid Commun Mass Spectrom 26:9–16

LaZerte BD (1983) Stable Carbon Isotope Ratios: Implications for the source of sediment carbon and for phytoplankton carbon assimilation in Lake Memphremagog Quebec. Can J Fish Aquat Sci 40(10): 1658–1666

Li S, Calmels D, Han G, Gaillardet J, Liu C (2008) Sulfuric acid as an agent of carbonate weathering constrained by $\delta^{13}C_{DIC}$: examples from Southwest China. Earth Planet Sci Lett 270:189–199

Li Q, He Y, Cao J, Liang J, Zhu M (2011a) The plant carbonic anhydrase at karst area and its ecological effects. Ecol Environ Sci 20:1867–1871

Li S, Lu X, He M, Zhou T, Bei R, Li L, Ziegler AD (2011b) Major element chemistry in the upper Yangtze River: a case study of the Longchuanjiang River. Geomorphology 129:29–42

Li R, Yu S, Sun P, He S, Yuan Y, Xiong Z (2015) Characteristics of $\delta^{13}C$ in typical aquatic plants and carbon sequestration by plant photosynthesis in the Banzhai catchment, Maolan of Guizhou Province. Carsol Sin 34:9–16

Lian B, Yuan D, Liu Z (2011) Effect of microbes on karstification in karst ecosystems. Sci Bull 56:3743–3747

Liu Z, Dreybrod W (1997) Dissolution kinetics of calcium carbonate minerals in H_2O-CO_2 solutions in turbulent flow: the role of the diffusion boundary layer and the slow reaction $H_2O+CO_2 \rightarrow H^+ + HCO_3^-$. Geochim Cosmochim Acta 61:2879–2889

Liu Z, Li Q, Sun H, Wang J (2007) Seasonal, diurnal and storm-scale hydrochemical variations of typical epikarst springs in subtropical karst areas of SW China: Soil CO_2 and dilution effects. J Hydrol 337:207–223

Liu Y, Zhang J, He Y, Sun H, Liu Z (2010) The utilization of dissolved inorganic carbon by *Oocystis solitaria wittr* and its influence on the precipitation of calcium carbonate. Geochimica 39:191–196

Liu Z, Dreybrodt W, Liu H (2011) Atmospheric CO_2 sink: silicate weathering or carbonate weathering? Appl Geochem 26(Supplement):S292–S294

Liu Z, Macpherson GL, Groves C, Martin JB, Yuan D, Zeng S (2018) Large and active CO_2 uptake by coupled carbonate weathering. Earth-Sci Rev 182:42–49

Maher K, Chamberlain CP (2014) Hydrologic regulation of chemical weathering and the geologic carbon cycle. Science 343:1502–1504

Martin JB (2017) Carbonate minerals in the global carbon cycle. Chem Geol 449:58–72

Mcconnaughey T (1998) Acid secretion, calcification, and photosynthetic carbon concentrating. Can J Bot 76:1119–1126

Négrel P, Allègre CJ, Dupré B, Lewin E (1993) Erosion sources determined by inversion of major and trace element ratios and strontium isotopic ratios in river water: the Congo Basin Case. Earth Planet Sci Lett 120:59–76

Pan G, He S, Cao J, Tao Y, Sun Y (2002) Variation of $\delta^{13}C$ in karst soil in Yaji Karst Experiment Site, Guilin. Sci Bull 47:500–503

Peng J, Hu R (2001) Carbon and oxygen isotope systematics in the Xikuangshan giant antimony deposit, central Hunan. Geol Rev 47: 34–41

Perrin AS, Probst A, Probst JL (2008) Impact of nitrogenous fertilizers on carbonate dissolution in small agricultural catchments: implications for weathering CO_2 uptake at regional and global scales. Geochim Cosmochim Acta 72:3105–3123

Pu J, Li J, Khadka MB, Martin JB, Zhang T, Yu S, Yuan D (2017) Instream metabolism and atmospheric carbon sequestration in a groundwater-fed karst stream. Sci Total Environ 579:1343–1355

Pu J, Li J, Zhang T, Martin JB, Khadka MB, Yuan D (2019) Diel-scale variation of dissolved inorganic carbon during a rainfall event in a small karst stream in southern China. Environ Sci Pollut Res 26: 11029–11041. https://doi.org/10.1007/s11356-019-04456-z

Qin X, Liu P, Huang Q, Zhang L (2013) Estimation of atmospheric/soil CO_2 consumption by rock weathering in the Pearl River Valley. Acta Geosci Sin 34:455–462

Raymond PA, Oh NH, Turner RE, Broussard W (2008) Anthropogenically enhanced fluxes of water and carbon from the Mississippi River. Nature 451:449–452

Redfield AC (1958) The biological control of chemical factors in the environment. Am Sci 46:230A–2221A

Roy S, Gaillardet J, Allègre CJ (1999) Geochemistry of dissolved and suspended loads of the Seine river, France: anthropogenic impact, carbonate and silicate weathering. Geochim Cosmochim Acta 63: 1277–1292

Sun H, Han J, Zhang S, Lu X (2007) The impacts of '05.6' extreme flood event on riverine carbon fluxes in Xijiang River. Sci Bull 52:805–812

Sun H, Han J, Li D, Zhang S, Lu X (2010) Chemical weathering inferred from riverine water chemistry in the lower Xijiang basin, South China. Sci Total Environ 408:4749–4760

Sun H, Han J, Zhang S, Lu X (2015) Carbon isotopic evidence for transformation of DIC to POC in the lower Xijiang River, SE China. Quat Int 380–381:288–296

Tao Z, Gao Q, Yao G, Shen C, Wu Q, Wu Z, Liu G (2004) The sources, seasonal variation and transported fluxes of the riverine particulate organic carbon of the Zengjiang River, Southern China. Acta Sci Circumst 24:789–794

Torres MA, West AJ, Li G (2014) Sulphide oxidation and carbonate dissolution as a source of CO_2 over geological timescales. Nature 507:346–349

Torres MA, West AJ, Clark KE (2015) Geomorphic regime modulates hydrologic control of chemical weathering in the Andes–Amazon. Geochim Cosmochim Acta 166:105–128

Turner RE, Rabalais NN (1991) Changes in Mississippi river water quality this century. Bioscience 41:140–147

Wang P, Cao J, Li L, Yang H, Li G (2013) Utilization of Ca^{2+} and HCO_3^- in karst water by chlorella from different sources. Acta Hydrob Sin 37(4):626–631

Wang P, Hu G, Cao J (2017) Stable carbon isotopic composition of submerged plants living in karst water and its eco-environmental importance. Aquat Bot 140:78–83

Waterson EJ, Canuel EA (2008) Sources of sedimentary organic matter in the Mississippi River and adjacent Gulf of Mexico as revealed by lipid biomarker and $\delta^{13}C_{TOC}$ analyses. Org Geochem 39:422–439

Wu Y, Xing D, Liu Y (2011) The characteristics of bicarbonate used by plants. Earth Environ 39(2):273–277

Wu Y, Xu Y, Li H, Xing D (2012) Effect of acetazolamide on stable carbon isotope fractionation in *Chlamydomonas reinhardtii* and *Chlorella vulgaris*. Chin Sci Bull 57:786–789

Xu Z, Liu C (2007) Chemical weathering in the upper reaches of Xijiang River draining the Yunnan–Guizhou Plateau, Southwest China. Chem Geol 239:83–95

Yang M, Liu Z, Sun H, Yang R, Chen B (2016) Organic carbon source tracing and DIC fertilization effect in the Pearl River: Insights from lipid biomarker and geochemical analysis. Appl Geochem 73:132–141

Yu S, He S, Sun P, Pu J, Huang J, Luo H, Li Y, Li R, Yuan Y (2016) Impacts of anthropogenic activities on weathering and carbon fluxes: a case study in the Xijiang River basin, southwest China. Environ Earth Sci 75:589

Zhang J, Quay PD, Wilbur DO (1995) Carbon isotope fractionation during gas-water exchange and dissolution of CO_2. Geochim Cosmochim Acta 59:107–114

Zhang S, Lu X, Higgitt DL, Chen C, Sun H, Han J (2007) Water chemistry of the Zhujiang (Pearl River): Natural processes and anthropogenic influences. J Geophys Res 112:F01011

Zhang C, Wang J, Pu J, Yan J (2012a) Bicarbonate daily variations in a Karst River: the Carbon sink effect of subaquatic vegetation photosynthesis. Acta Geol Sin Engl Ed 86:973–979

Zhang H, Yu S, He S, Liu Q, Li Y (2012b) Analysis on the chemical characteristics of the atmospheric precipitation in Guilin. Carsol Sin 31:289–295

Zhang C, Xie Y, Ning L, Yu H, Wang J, Li F (2013) Characteristics of $\delta^{13}C$ in typical aquatic plants and carbon sequestration in the Huixian karst wetland, Guilin. Carsol Sin 32:247–252

Zhou J (2015) Climate, depositional environmental changes from middle Holocene to the present documented in Guilin karst wetland. Southwest University, Chongqing

Zhou Z, Chen C, Liu K, Li J, Chen M, Jiang Y, Yu F (2014) Phytoplankton community and water quality in Guilin city section of Lijiang River in summer, China. Ecol Environ Sci 23:649–656